63 MeV Proton Beam Profile Monitoring with Radioluminescent Ce-doped Optical Fiber Sensor

J. Vidalot, A. Morana, O. Duhamel, C. Hoehr, H. El Hamzaoui, A. Boukenter, Géraud Bouwmans, Andy Cassez, B. Capoen, M. Trinczek, et al.

63 MeV Proton Beam Profile Monitoring with Radioluminescent Ce-doped Optical Fiber Sensor

J. Vidalot, A. Morana, *Member IEEE,* O. Duhamel, C. Hoehr, H. El Hamzaoui, A. Boukenter, G. Bouwmans, A. Cassez, B. Capoen, M. Trinczek, *Member IEEE,* Y. Ouerdane, P. Paillet, *Fellow IEEE,* M. Gaillardin, *Member, IEEE,* M. Bouazaoui, and S. Girard, *Senior Member, IEEE*

***Abstract*- We investigated the potential of an optical material (Ce-doped silica rod of ~0.5 mm in diameter and ~1 cm in length) developed by sol-gel process to perform *in situ* proton beam profile measurement through the monitoring of its visible radioluminescence features peaking around 480 nm. Various test configurations (collimator sizes and varying distances from the collimators) have been performed to assess the sensor performances at the TRIUMF facility in Vancouver offering a 63 MeV proton beam. The obtained results are promising, showing their potential to characterize the flux and beam profile at this facility offering radiation testing capabilities or medical treatments. The reported performances could be improved by pre-irradiating the probe sample to reduce the observed slight Bright Burn effect on the quality of the profile measurements. These results open the way to most advanced sensors architecture such as ribbons of optical fibers drawn from this sol-gel rod, to acquire in one step the complete beam profile.**

***Index Terms*—Radiation effects, Optical Materials, radio-luminescence, Optical Fibers, Protons, Beam monitoring**

I. Introduction

Nowadays, many applications exploiting particle beams require a strong knowledge about their flux and profile to achieve the needed irradiation goals. In radio-, proton- and hadron-therapy applications as well as for radiation testing of microelectronic or photonic devices, measuring the beam profile is both a requirement and a safe practice.

Manuscript received xxx.

J. Vidalot, A. Morana, A. Boukenter, Y. Ouerdane and S. Girard are with Université Jean Monnet, CNRS 5516, IOGS, Laboratoire Hubert Curien, F-42000 Saint Etienne, France: phone (33) 4 77 91 58 14; e-mail: jeoffray.vidalot@univ-st-etienne.fr ; sylvain.girard@univ-st-etienne.fr.

O. Duhamel and P. Paillet are with CEA, DAM, DIF, F-91297 Arpajon, France.

H. El Hamzaoui, G. Bouwmans, A. Cassez, B. Capoen and M. Bouazaoui, are with Univ-Lille, CNRS, UMR8523 - PhLAM – Physique des Lasers, Atomes et Molécules, CERLA/IRCICA, F-59000 Lille, France: (mohamed.bouazaoui@univ-lille1.fr)

C. Hoehr and M. Trinczek, are with TRIUMF, Vancouver, Canada (e-mail: trinczek@triumf.ca)

M. Gaillardin is with CEA, CEG, Gramat, France

Several detector technologies, such as ion chambers, radiochromic films or scintillating materials in a phantom, can be used to evaluate the particle flux, the beam spatial distribution and homogeneity [1]–[5]. The current challenge consists in simultaneously developing *in situ and real-time* technologies, optimizing the flux measurement, decreasing the monitor cost and increasing its spatial resolution to cover the increasing needs in terms of microscale dosimetry. In the last decade, optical fibers have shown their capabilities to be implemented in the harsh environments of high energy physics facilities, nuclear power plants and nuclear waste repositories [6]–[8]. Under proton exposure, two main radiation effects (*Radiation-Induced Attenuation (RIA), Radiation-Induced Emission (RIE))* have been reported on optical materials and optical fibers [8]. While most efforts have focused on the mitigation of these macroscopic radiation effects, they can also be exploited to develop radiation detectors, beam instrumentation or even dosimeters. Their benefits can be exploited through the fiber's small size, low weight, electromagnetic immunity and the possibility to delocalize the acquisition system in radiation-free instrumentation zone.

ACKNOWLEDGEMENTS

TRIUMF receives federal funding via a contribution agreement with the National Research Council of Canada.

H. El Hamzaoui, G. Bouwmans, A. Cassez, B. Capoen and M. Bouazaoui would like to acknowledge FiberTech Lille platform for its technical support. This work was supported in part by the Agence Nationale de la Recherche through LABEX CEMPI (ANR-11-LABX-0007). This work was also carried out within the framework of the Contrat de Plan Etat-Region (CPER) WaveTech, which is supported by the Ministry of Higher Education and Research, the Hauts-de-France (HdF) Regional council, the Lille European Metropolis (MEL), the Institute of Physics of the French National Centre for Scientific Research (CNRS) and the European Regional Development Fund (ERDF).

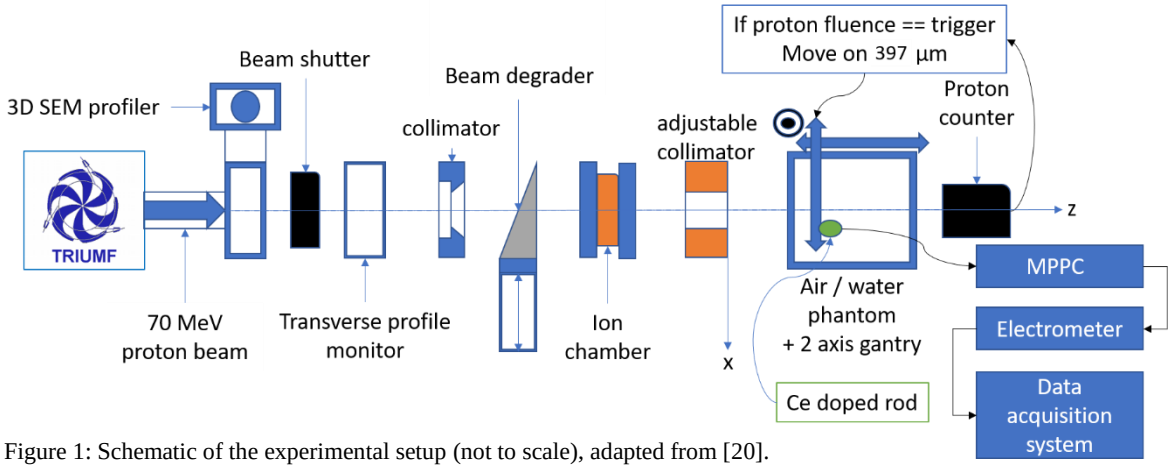

Figure 1: Schematic of the experimental setup (not to scale), adapted from [20].

RIA corresponds to an opacification of the optical material exposed to radiation: the glass transmission decreases. The degradation amplitudes and kinetics depend on many intrinsic (material-related) and extrinsic parameters linked to the irradiation conditions: the particle type, flux, fluence and temperature of irradiation. At the microscopic scale, when the silica-based glass or optical fiber is irradiated, precursor sites can be converted into optically-active defects or Si-O-Si bonds can be broken by ionization or knock-on processes, leading to radiation-induced point defects [9]. Each center is characterized by its own absorption bands, which degrade the fiber transmission giving rise up to RIA. Furthermore, a fraction of these defect structures are also associated with luminescence bands in the ultraviolet and visible domains [9]. It is worth noticing that the fiber RIA response under radiation strongly depends on the glass composition that drives the natures and the concentrations of the radiation-induced defects and then their optical properties. Several studies showed that the RIA can be used for real-time dosimetry: for example, incorporating phosphorous in the fiber core leads to a radiation response suitable for dosimetry, as shown under electrons, neutrons, protons, X-ray or γ-ray beams [10]–[12].

The second phenomenon of interest for radiation dosimetry is RIE. It encompasses both Cerenkov and non-Cerenkov light emissions under exposure. In one hand, Cerenkov radiation [13] is produced by relativistic charges passing through the material with a velocity higher than the light phase velocity. So, produced by primary or secondary charges, an electromagnetic wave is generated in the medium propagating in the same direction than the incoming charge. In our case, Cerenkov radiation generation is led by secondary electrons produced during proton-silica atoms interaction when ionized electrons have a kinetic energy higher than 186 keV for silica refractive index of 1.46 [14]. The Cerenkov photon flux linearly depends on the incoming particle flux with an angular distribution inversely function of the reduced particle velocity β (v/c with v the particle velocity and c the light celerity in vacuum) as observed in many experiments oriented to dosimetry applications [15], [16]. The light spectrum is inversely proportional to the square of the wavelengths from the visible to the near ultraviolet [14]–[16]. To assist Cerenkov radiation and amplify radiation detection, radioluminescence (RIL) can be exploited to design radiation monitors or even dosimeters if a calibration is possible. For such a sensor, a highly sensitive detector is selected to monitor in situ the RIL fluctuations. The RIL basic principle, of interest for this work, is illustrated in [17], [18] for the case of the Ce-doped silica glass also well described by scintillation mechanism [19].

Previous studies have shown that for some optical materials, the RIL and RIE signals linearly depend on the particle flux. It then enables a real-time monitoring of the particle flux variation [20]. For radio- and proton-therapy, the rods or optical fiber materials made by sol-gel process doped with Cerium (Ce), Gadolinium (Gd), and Copper (Cu) have exhibited very interesting properties [9], [21]–[26]. Moreover, it has been demonstrated that all these materials can be drawn into optical fibers of core size down to a few micrometers. The interest for this technology is explained by the possibility to develop miniature sensors, leading to high spatial resolution flux or fluence mapping at potentially moderate manufacturing cost [27], [28]. In this article, we focus on Ce-doped optical rod, previously characterized in [22], [29], to perform real-time profile measurements of the 63 MeV proton beamline at the TRIUMF facility [30].

II. Experimental Procedure

The experimental setup, as illustrated in Figure 2, was installed in the TRIUMF proton irradiation facility at Vancouver (Canada) [31]. One of its two beamlines can deliver protons with an energy available from 5 to 120 MeV with a beam current of 6 nA for our experiment. For therapy applications, the proton energy is reduced to 63 MeV by a degrader and the initial beam size is quite small (~8 mm Full Width at Half Maximum (FWHM)). To enable radiation testing with a homogeneous beam field, the proton beam size was

spread by targeting a thick lead disk. The beam diameter was thus increased from 8 to 7 cm. To optimize the radiation tests, the proton beam size is usually adjusted with a metallic collimator. We used three collimator sizes: 8×8 mm², 8×12 mm² and 8×16 mm² respectively, with the largest dimension in the horizontal plan transverse to the beam. After the collimator, the transverse shape of the beam corresponded to a rectangle in which the rod under test was located. As illustrated in Figure 2, the rod was fixed on a PMMA support, which was mounted on a 3-axis motorized gantry with remote control, allowing the rod displacement within the beam directly from the control room. During our experiments, only two axes were switched on, the longitudinal axis along the beam (defined as the z-axis) and the transverse axis across the beam (defined as the x-axis). The y axis was not used as the sensor has an extended size in that direction. The sensor performance was assessed at three distances from the collimator (positions along the z-axis). The response of the Ce-doped rod RIE was measured at 10, 14 and 22 cm from the collimator. Along the x-axis, a scan was performed with a 396.9 µm step, covering the range for each collimator size. For the RIE measurements, one extremity of the rod was spliced to a radiation-resistant transport multimode (MM) optical fiber connected to a Multi-Pixel Photon Counter (MPPC, Hamamatsu, model C11208-01(X) [32]). At the MPPC, the radioluminescence produced by the sample was converted into photo-electrons that are amplified and then counted by the calibrated electrometer at the TRIUMF acquisition system. The x-axis step motor performs a remotely-controlled scan: at each step position, the time gate was equivalent to the needed time to record a proton fluence calibrated at TRIUMF facility [33] of 1000 Monitor Count (MC) into the detector. For our experiment, TRIUMF facility has calibrated the dose deposited per 1 MC of 63 MeV proton fluence with the following conversion factor: 1 MC = 8.5 10^{-5} Gy(SiO_2).

The Ce-doped rod was prepared through a sol-gel process. This sample consists of a small glass cylinder with a diameter of ~0.5 mm and a length of ~1 cm, doped with Ce^{3+} ions. The rod was manufactured in the technological platform FiberTech Lille (France), and spliced to a 500 µm multimode pure silica core fiber, necessary to transport the RIE signal to the PMT. This doped rod has already shown very interesting results for proton therapy applications [22]. Figure 2 shows the RIL spectrum acquired under the 63 MeV protons irradiation using a spectrometer (QE65000 from Ocean Optics). It consists of one large band peaking around 480 nm. This signature is similar to the one previously obtained under X-rays [25], [34] and is typical of Ce^{3+} ions, incorporated in silica based rods or optical fibers.

It is possible to note from these measurements that the contribution of the Cerenkov emission is negligible compared to the sample RIL in our test conditions. This agrees with previous study [29] showing that Cerenkov accounts for less than one percent of the RIE for a 63 MeV proton beam. We can then consider in this work that the recorded signal is only related to the RIL from the Ce^{3+} ions. However, RIE ~~as~~ denomination will be used hereafter for light emission coming from irradiated Ce doped rod. The same type of RIL/RIE spectral measurement had been previously performed on similar Ce-doped rods [25], [26], [29] under 40 keV X-rays, 6 MV electron and ^{60}Co gamma photon beams. The samples always showed equivalent features, confirming the good agreement with the present spectrum performed under 63 MeV proton beam.

The RIE intensities of this rod exhibited a linear dependence versus the proton flux, as highlighted in Figure 3, which validates the use of the rod for beam profile monitoring in this range of flux [22], [29]. Due to the temperature dependence of RIE [35] (an increase of ~70% of the light ouput over the -120°C to 20°C range), it should be specified that the experiments have been performed at room temperature around 22 °C.

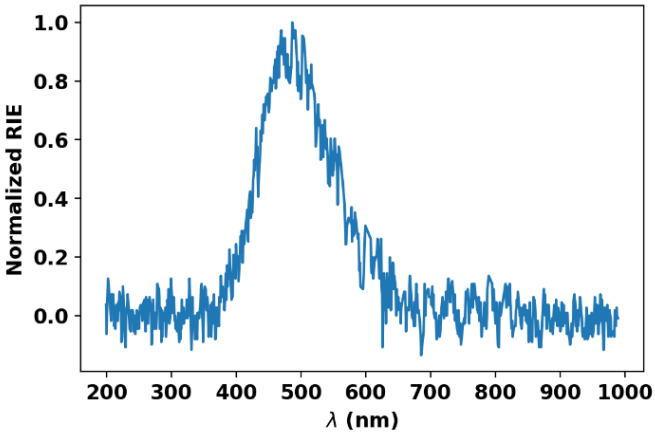

Figure 2: 63 MeV proton RIL spectrum for the Ce doped rod.

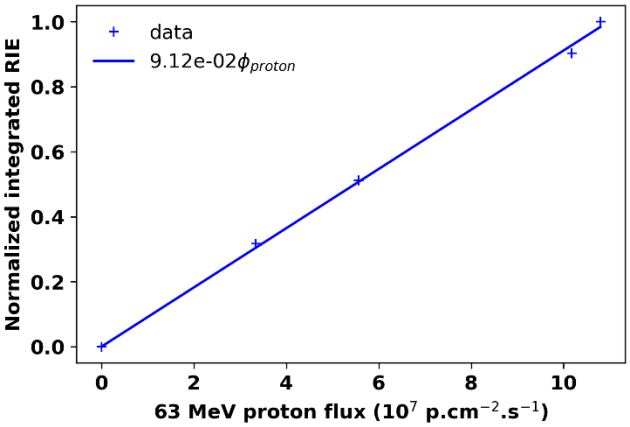

Figure 3: Linear dependence of the radioluminescence of the Ce-doped sample against the 63 MeV proton beam flux.

In order to determine the characteristics of the collimated beams, the raw data had to be post-processed which is actually performed at TRIUMF facility. First, when the PMT is switched ON in the absence of radiations, the device dark current and the optical noise (*small amount of ambient light is still detected by the PMT*) introduce a background noise, which

is evidenced as the first baseline on the left part of the raw signal and that should be removed. The level of the dark current was taken at the minimum of the signal. Similarly, the baseline at the right side of the signal had to be considered as part of the background as well. To treat the background noise, we defined a minimum threshold on the foot of the signal equal on both sides. Then, all the signal which was below it was removed while above was considered as RIE signal. The intensity difference between the two sides may be explained by the post-irradiation radioactive background produced by the primary irradiation activation which interacts with the RIE rod and produces a post irradiation luminescent background. This phenomenon is convoluted to the effects induced by the movement of the rod into a radioactive environment. From the raw data, the background was selected between the scan limits and before the onset of the RIE signal induced by the primary beam irradiation. Then, the full background was fitted. This complete background was subtracted to each data, giving the data shown in Figure **4**.

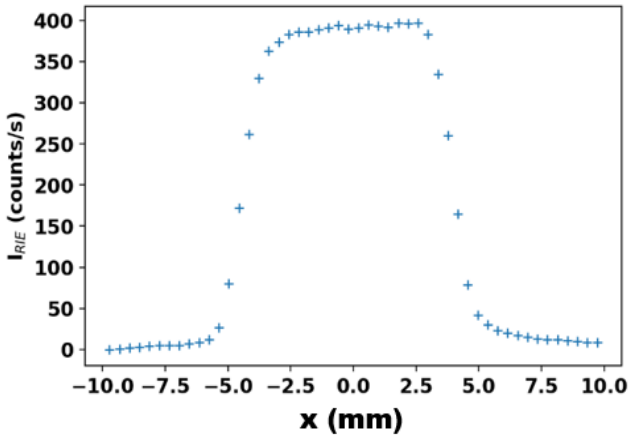

Figure 4: Processed data for the Ce-doped rod located at 10 cm from the 8×8 mm² collimator.

Once the background was removed, an interpolation method was applied to transform the discrete raw data into a continuous form, which enables the extraction of different information from the processed data. The most crucial parameter for protontherapy applications is the full width at half maximum (FWHM) of the RIE signal. This value is directly related to the accuracy and reliability of the sample used for the beam profile monitoring as it is a measure of the beam size at different collimator sizes. This FWHM is also of interest for radiation testing to better assess the homogeneity of the beam with respect to the device under test. The second information which can be extracted is the profile asymmetry. To study it, we extracted from the processed data the distance variation between the x positions at 20% and 80% of the maximum for the left-hand and hand-hand penumbra of the plateau (i.e. the rise and fall distances of the signal). The difference between the two distances reveals the asymmetry of the beam profile caused by the detector as it is known that the TRIUMF beam is symmetric. This difference should reach a limit which should correspond to the convolution between the rod dimension and the beam penumbra size. However, due to the slope of the top-hat baseline, the estimation of the FWHM only from the maximum of the RIE signal would be a wrong method to evaluate the values of interest. The maximum of each data series could be associated to a fluctuation of the signal from a dark current peak. For this reason, two different analysis methods were performed. The first one considered the maximum of the RIE signal after background substracting. For the second analysis, a fit of the slope of the signal was applied to calculate the signal average as reference for the FWHM evaluation. The measured signal is a convolution between the temporal effects due to the proton flux at each position and the following of the proton beam current evolution. Due to the multiple exposures of the rod to the proton beam, we have to consider the possible generation of additional absorbing or emitting color centers. If the proton beam current is stable during the displacement of the rod under irradiation, the top should be flat. No noticeable radiation-induced attenuation was expected for the sol-gel materials at the considered fluences. Indeed, RIA should lead to a decreasing slope for the plateau and an opposite behavior was actually observed. Whereas, at the maximum proton fluence, namely on the RIE plateau, the accumulated dose in one RIE point was 0.85 Gy(SiO_2), given a total ionizing dose (TID) on the plateau of about 15 Gy(SiO_2). Yet, previous articles [29], [36], [37], reporting equivalent dose deposition in Ce-doped fibers or rods, did not mention any RIA effect. However, many effects could contribute to explain this increasing plateau. As an example, radiation could induce new radioluminescent defects, which add intensity to the base-level due to the precursor sites.

III. Results and Discussion

A. TRIUMF FWHM Processing Based Study

All the data shown in this section have been processed and normalized to the maximum of each data set. The beam profile is shown in Figure 5 for the three collimator sizes at three respective distances from the collimator (Figure 5--(a, b, c)).

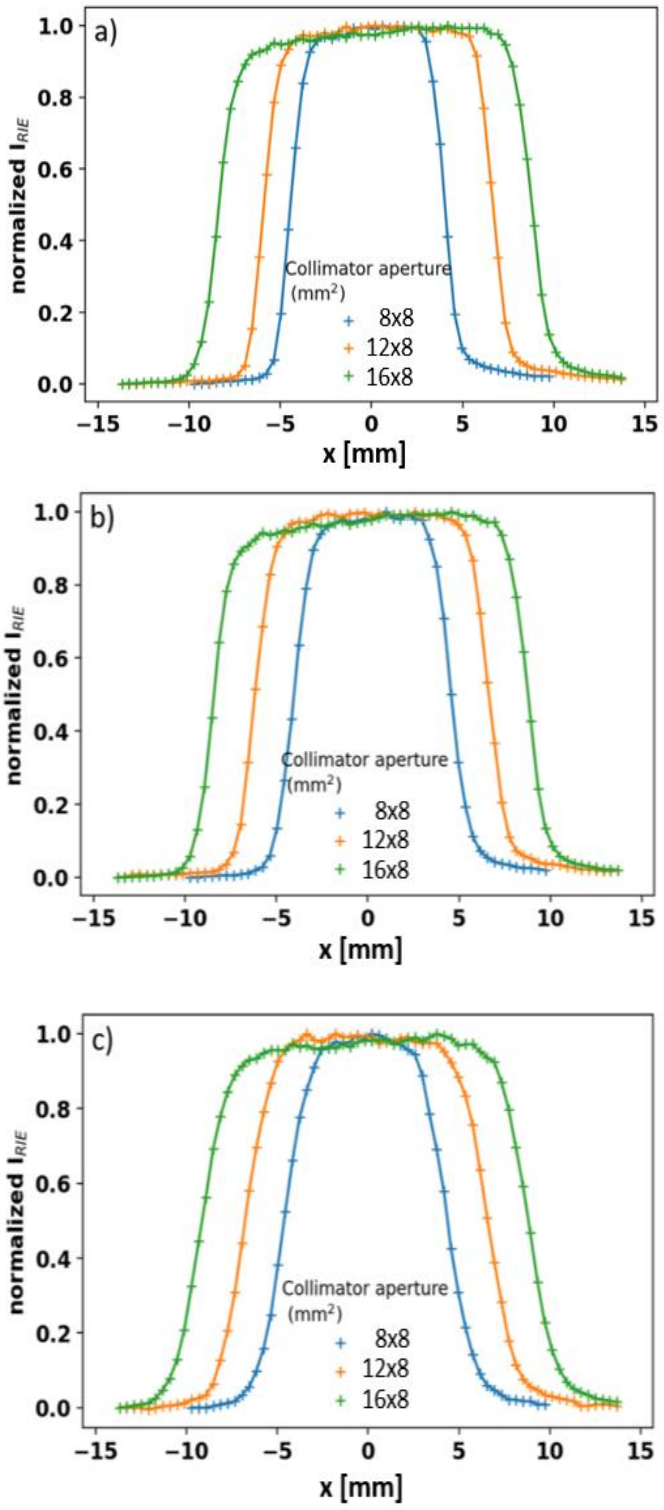

Figure 5: Beam profiles as measured with the Ce-doped rod for all three collimator sizes (blue line: 8×8 mm², orange line: 12×8 mm², green line: 16×8 mm²) at a distance of 10 cm (a), 14 cm (b), and 22 cm (c) from the collimator.

TABLE 1. FWHM (IN MM) MEASURED WITH THE CE-DOPED ROD FOR ALL COLLIMATORS AT 3 DIFFERENT DISTANCES.

		Distance from the collimator		
		10 cm	14 cm	22 cm
Collimator size (mm²)	8×8	8.14 ± 0.8	8.62 ± 0.8	8.56 ± 0.8
	12×8	12.68 ± 0.8	12.81 ± 0.8	12.79 ± 0.8
	16×8	16.81 ± 0.8	17.18 ± 0.8	17.18 ± 0.8

Table 1 summarizes the RIE signal FWHM for all the beams, varying both the collimator size and the collimator-rod distance. The FWHM error is the absolute difference between the calculated FWHM and profile width measured just lower than the half of the maximum. The measurements are consistent with the expected beam profiles.

Nevertheless, even with all background subtracted the beam plateau is not perfectly flat, as can be seen in Figure 6. This could be explained by the secondary radiation induced effects known as Bright Burn Effect [38], [39]. This can also be due to electron trapping in defect states more stable than those producing the RIL [36]. The result in our data is an increase of almost 10% of the signal during the irradiation with a TID of about 15 Gy(SiO_2). In [36] for instance, the RIE increased of about 5 % at room temperature over almost 6 Gy(SiO_2), which is comparable with our results. The last section of this article will be dedicated to investigate this effect. The negligible evolution of the FWHM with distance from the collimator shows that the divergence of the beam after collimation remains small, thereby confirming the collimator keeps beam size stable over the distance for radiation testing. This FWHM evaluation method reaches a limit regarding the possibility to measure the proton beam dispersion through a distance from the collimator. Indeed, between 14 and 22 cm, the FWHM seems diverging which should be expected over the distance. A second method is proposed next to this one to better evaluate the FWHM.

For each side of the plateau, the distance between points located at 20% and 80% of the maximum the penumbra size, is measured. The difference between left-side and right-side distances, reported in Table 2, is a measurement of the beam asymmetry. This is also a critical issue from the protontherapy standpoint, less critical for radiation testing more focused on integrated fluence. If an asymmetry exists, the irradiation does not deliver the expected dose and the treatment might be misevaluated by our sensor.

TABLE 2: SUMMARY OF THE ASYMMETRY BETWEEN THE LEFT AND RIGHT SIDES OF THE PLATEAU (IN m

m)

		Distance from the collimator		
		10 cm	14 cm	22 cm
Collimator size (mm²)	8×8	0.12	0.03	0
	12×8	0.12	0.07	0.09
	16×8	0.15	0.19	0.14

B. TOP AVERAGING BASED STUDY

As explained before, the data set analyzed in this section is the fitted background-subtracted data. In this subsection, the same analyses are performed on the data taking the mean of the plateau as the reference for the calculation of the FWHM and the asymmetry. The data used to average the signal is selected by a threshold condition where all the values above 87% of the signal maximum are considered as the top. The threshold is the limit between the RIE rise up and the RIE plateau. FWHM and the asymmetry are studied taking this mean value as the maximum.

TABLE 3: REEVALUATED FWHM (IN mm) FOR ALL COLLIMATORS AT 3 DIFFERENT DISTANCES TAKING THE PLATEAU AVERAGE AS A REFERENCE

		Distance from the collimator		
		10 cm	14 cm	22 cm
Collimator size (mm²)	8x8	8.2	8.54	8.61
	12x8	12.63	12.69	12.85
	16x8	16.85	17.04	17.24

Table 3 summarizes the RIE signal FWHM for all the beams evaluated from the mean value of the top hat form, varying both the collimator size and the collimator-rod distance. This second method reveals some differences in the evaluation of the FWHM. The use of an average as reference for the calculation of the FWHM brings a stability of this parameter. The main effect is to remove the fluctuation which might be a source of misevaluation of the reference, and by extension, of the FWHM value. The differences of reproducibility of the size of longitudinal dimension of the profile are reduced but the relative difference between the values reported in Table 1 and Table 3 at equivalent parameters becomes more homogeneous around 1%. The evolution in the asymmetry differences is also shown in Table 4 where the distances seem more regular than in Table 2. Finally, this new method brings observation about the divergence of the proton beam over the distance misevaluated with the previous method.

From the fit method applied to the data, the mean error on the values are linked to the measurement step, which is larger than the fitting mesh precision, while remaining below 5%.

TABLE 4: SUMMARY OF THE REEVALUATED ASYMMETRY BETWEEN LEFT AND RIGHT SIDES OF THE PLATEAU (IN mm) USING THE AVERAGE METHOD.

		Distance from the collimator		
		10 cm	14 cm	22 cm
Collimator size (mm²)	8x8	0.08	0.03	0.03
	12x8	0.05	0.03	0.03
	16x8	0.09	0.1	0.06

C. INCREASE OF RIE DURING PROTON IRRADIATION

To further investigate the asymmetry of the RIE plateau observed in each beam profile scan of Figure 6, reverse scans of the beam have been performed by reversing the motor progression direction. As illustrated in Figure 6, the RIE signal increase essentially occurs during the direct scan. This gives to the Bright Burn Effect a major role in the RIE increase phenomenon, rather than a rod tilt effect because of the quasi-symmetry of the RIE evolution in the reverse excursion.

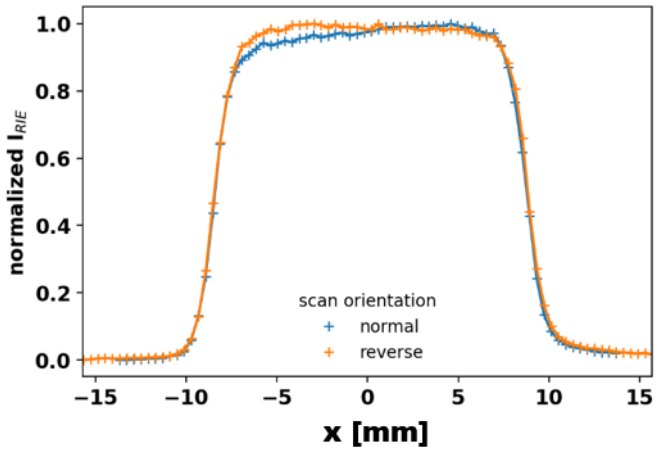

Figure 6: RIE measured during normal (blue crossed line) and reverse (orange crossed line) scan made with the Ce doped rod.

Due to short irradiation times (< few minutes), the RIE increase remains limited to a few percent of the total RIE amplitude. Moreover, the direct impact of the initial top-hat shape asymmetry is on the RIE plateau maximum, but as seen from Figure 7, it has almost no influence on the FWHM calculation. Indeed, the two scan are superimposed in the Figure 6 during the increase and the decrease of the signal. From this observation, a pre-irradiation process of the sensing probes could lead to a reduction of this effect, as already observed in previous investigations of radioluminescent fibers for dosimetry applications [40], [41].

IV. Conclusions

A Ce-doped silica rod appears as a very promising sensing solution for beam monitoring, as shown by our tests on its capability to measure the 63 MeV proton beam profiles using different collimator sizes at the TRIUMF facility. This new kind of detector exhibits high precision 63 MeV proton beam profile measurement based on rectangle shape collimator. For all RIE profile measured with a set of three collimators and three distances for the collimator, Ce doped rod becomes competitive with commercial detector. This is additioned with a new data processing technique able to increase measurement accuracy for proton beam width evaluation as well as beam divergence small in this case as observed by the current results. For some medical applications like radio- and proton-therapy, drawing the tested rod into optical fibers with even more reduced size, with sensitive doped core of a few tens of microns, should lead to very high spatial accuracy measurements. Furthermore, we can imagine multiplying the number of fibers in the form of a planar bundle in order to simultaneously record the proton flux at various locations of the beam. This kind of achievements may pave the way to a time-resolved mapping of the beam profile for specific needs. Additional experiments should be performed with other kinds of particles like neutrons or electrons to study the rod particle sensitivity and its potential for beam profile monitoring. To also adapt and extend the proton beam flux range, this method could be explored with different sizes of optical fiber by adjusting the doped region diameter, changing the dopant for a more sensitive radioluminescent element and the concentration of dopant. Moreover, this detector could be assisted by a metal mirror which could collect RIE photons progressing in the non-instrumented direction of the fiber probe, as already investigated for low energy X-ray beam [41]. Finally, repeatability of RIE profile has been shown here on multiple scans but should be further investigated to determine the impact of ionizing radiation dose accumulated scan after scan and during longer irradiation runs.

References

[1] S. Giordanengo, L. Manganaro, and A. Vignati, “Review of technologies and procedures of clinical dosimetry for scanned ion beam radiotherapy,” *Phys. Med.*, vol. 43, pp. 79–99, Nov. 2017, doi: 10.1016/j.ejmp.2017.10.013.

[2] I. J. Yeo, A. Teran, A. Ghebremedhin, M. Johnson, and B. Patyal, “Radiographic film dosimetry of proton beams for depth-dose constancy check and beam profile measurement,” *J. Appl. Clin. Med. Phys.*, vol. 16, no. 3, pp. 318–328, 2015, doi: 10.1120/jacmp.v16i3.5402.

[3] S. H. Kim, J. W. Lee, W. S. Jung, J. K. Ahn, M. H. Jung, and Y. J. Kim, “Three-dimensional measurement of a proton beam profile at KOMAC with a scintillating fiber detector,” *Nucl. Instrum. Methods Phys. Res. Sect. Accel. Spectrometers Detect. Assoc. Equip.*, vol. 1034, p. 166832, Jul. 2022, doi: 10.1016/j.nima.2022.166832.

[4] J. Bosser, J. Mann, G. Ferioli, and L. Warts, “Optical transition radiation proton beam profile monitor,” *Nucl. Instrum. Methods Phys. Res. Sect. Accel. Spectrometers Detect. Assoc. Equip.*, vol. 238, no. 1, pp. 45–52, Jul. 1985, doi: 10.1016/0168-9002(85)91025-3.

[5] N. Kumar *et al.*, “Non-invasive beam profile monitor for medical accelerators,” *Phys. Medica PM Int. J. Devoted Appl. Phys. Med. Biol. Off. J. Ital. Assoc. Biomed. Phys. AIFB*, vol. 73, pp. 173–178, May 2020, doi: 10.1016/j.ejmp.2020.04.023.

[6] H. T. Zubair *et al.*, “Real-time radiation dosimetry using P-doped silica optical fiber,” *Measurement*, vol. 146, pp. 119–124, Nov. 2019, doi: 10.1016/j.measurement.2019.06.010.

[7] S. Delepine-Lesoille *et al.*, “France’s State of the Art Distributed Optical Fibre Sensors Qualified for the Monitoring of the French Underground Repository for High Level and Intermediate Level Long Lived Radioactive Wastes,” *Sensors*, vol. 17, no. 6, Art. no. 6, Jun. 2017, doi: 10.3390/s17061377.

[8] S. Girard *et al.*, “Radiation Effects on Silica-Based Optical Fibers: Recent Advances and Future Challenges,” *IEEE Trans. Nucl. Sci.*, vol. 60, no. 3, pp. 2015–2036, Jun. 2013, doi: 10.1109/TNS.2012.2235464.

[9] S. Girard *et al.*, “Overview of radiation induced point defects in silica-based optical fibers,” *Rev. Phys.*, vol. 4, p. 100032, Nov. 2019, doi: 10.1016/j.revip.2019.100032.

[10] D. D. Francesca *et al.*, "Qualification and Calibration of Single-Mode Phosphosilicate Optical Fiber for Dosimetry at CERN," *J. Light. Technol.*, vol. 37, no. 18, pp. 4643–4649, Sep. 2019, doi: 10.1109/JLT.2019.2915510.

[11] S. Girard, Y. Ouerdane, C. Marcandella, A. Boukenter, S. Quenard, and N. Authier, "Feasibility of radiation dosimetry with phosphorus-doped optical fibers in the ultraviolet and visible domain," *J. Non-Cryst. Solids*, vol. 357, no. 8, pp. 1871–1874, Apr. 2011, doi: 10.1016/j.jnoncrysol.2010.11.113.

[12] S. Girard *et al.*, "Atmospheric Neutron Monitoring through Optical Fiber-Based Sensing," *Sensors*, vol. 20, no. 16, Art. no. 16, Jan. 2020, doi: 10.3390/s20164510.

[13] G. N. Afanasiev, V. G. Kartavenko, and Y. P. Stepanovsky, "On Tamm's problem in the Vavilov-Cherenkov radiation theory," *J. Phys. Appl. Phys.*, vol. 32, no. 16, p. 2029, Aug. 1999, doi: 10.1088/0022-3727/32/16/311.

[14] J. Wolfenden *et al.*, "Cherenkov Radiation in Optical Fibres as a Versatile Machine Protection System in Particle Accelerators," *Sensors*, vol. 23, no. 4, Art. no. 4, Jan. 2023, doi: 10.3390/s23042248.

[15] E. Ciarrocchi and N. Belcari, "Cerenkov luminescence imaging: physics principles and potential applications in biomedical sciences," *EJNMMI Phys.*, vol. 4, no. 1, p. 14, Mar. 2017, doi: 10.1186/s40658-017-0181-8.

[16] K. W. Jang *et al.*, "Feasibility of fiber-optic radiation sensor using Cerenkov effect for detecting thermal neutrons," *Opt. Express*, vol. 21, no. 12, pp. 14573–14582, Jun. 2013, doi: 10.1364/OE.21.014573.

[17] R. Chen and V. Pagonis, *Advances in Physics and Applications of Optically and Thermally Stimulated Luminescence*. 2018. doi: 10.1142/q0172.

[18] N. Alhelou, "Etude de verres pour la dosimétrie fibrée de rayonnements ionisants," These de doctorat, Université de Lille (2018-2021), 2018. Accessed: Apr. 29, 2022. [Online]. Available: http://www.theses.fr/2018LILUR032

[19] P. Lecoq, A. N. Annenkov, A. Gektin, M. Korzhik, and C. Pédrini, *Inorganic Scintillators for Detector Systems: Physical Principles and Crystal Engineering; 1st ed.* in Particle acceleration and detection. Berlin: Springer, 2006. doi: 10.1007/3-540-27768-4.

[20] S. Girard *et al.*, "Potential of Copper- and Cerium-Doped Optical Fiber Materials for Proton Beam Monitoring," *IEEE Trans. Nucl. Sci.*, vol. 64, no. 1, pp. 567–573, Jan. 2017, doi: 10.1109/TNS.2016.2606622.

[21] N. Al Helou, "Etude de verres pour la dosimétrie fibrée de rayonnements ionisants," These de doctorat, Université de Lille (2018-2021), 2018. Accessed: May 22, 2023. [Online]. Available: https://www.theses.fr/2018LILUR032

[22] "Potential of Copper- and Cerium-Doped Optical Fiber Materials for Proton Beam Monitoring | IEEE Journals & Magazine | IEEE Xplore." Accessed: May 22, 2023. [Online]. Available: https://ieeexplore.ieee.org/document/7562459

[23] C. Hoehr *et al.*, "Novel Gd3+-doped silica-based optical fiber material for dosimetry in proton therapy," *Sci. Rep.*, vol. 9, no. 1, Art. no. 1, Nov. 2019, doi: 10.1038/s41598-019-52608-5.

[24] J. Bahout *et al.*, "Cu/Ce-co-Doped Silica Glass as Radioluminescent Material for Ionizing Radiation Dosimetry," *Materials*, vol. 13, no. 11, Art. no. 11, Jan. 2020, doi: 10.3390/ma13112611.

[25] A. Vedda *et al.*, "Ce3+-doped fibers for remote radiation dosimetry," *Appl. Phys. Lett.*, vol. 85, no. 26, pp. 6356–6358, Dec. 2004, doi: 10.1063/1.1840127.

[26] E. Mones *et al.*, "Ce-doped optical fibre as radioluminescent dosimeter in radiotherapy," *Radiat. Meas.*, vol. 43, no. 2, pp. 888–892, Feb. 2008, doi: 10.1016/j.radmeas.2008.01.031.

[27] H. E. Hamzaoui *et al.*, "Sol-gel derived ionic copper-doped microstructured optical fiber: a potential selective ultraviolet radiation dosimeter," *Opt. Express*, vol. 20, no. 28, pp. 29751–29760, Dec. 2012, doi: 10.1364/OE.20.029751.

[28] B. Capoen *et al.*, "Innovative copper-doped glasses and fibers as sensitive materials for ionizing beam dosimetry," Aug. 2015. Accessed: May 22, 2023. [Online]. Available: https://hal.science/hal-01198825

[29] D. Söderström *et al.*, "Radioluminescence Response of Ce-, Cu-, and Gd-Doped Silica Glasses for Dosimetry of Pulsed Electron Beams," *Sensors*, vol. 21, no. 22, Art. no. 22, Jan. 2021, doi: 10.3390/s21227523.

[30] G. C. Ball, G. Hackman, and R. Krücken, "The TRIUMF-ISAC facility: two decades of discovery with rare isotope beams," *Phys. Scr.*, vol. 91, no. 9, p. 093002, Jul. 2016, doi: 10.1088/0031-8949/91/9/093002.

[31] "Proton Irradiation Facility (PIF) Overview | TRIUMF : Canada's particle accelerator centre." Accessed: May 22, 2023. [Online]. Available: https://www.triumf.ca/proton-irradiation-facility

[32] "Photosensor module H9305-13 | Hamamatsu Photonics." Accessed: May 22, 2023. [Online]. Available: https://www.hamamatsu.com/eu/en/product/optical-sensors/pmt/pmt-module/current-output-type/H9305-13.html

[33] C. Penner, C. Hoehr, C. Lindsay, C. Duzenli, and S. O'Keeffe, "Timing resolution for an optical fibre-based detector in a 74 MeV proton therapy beam," *J. Phys. Conf. Ser.*, vol. 1067, no. 6, p. 062001, Sep. 2018, doi: 10.1088/1742-6596/1067/6/062001.

[34] N. Al Helou *et al.*, "Radioluminescence and Optically Stimulated Luminescence Responses of a Cerium-Doped Sol-Gel Silica Glass Under X-Ray Beam Irradiation," *IEEE Trans. Nucl. Sci.*, vol. 65, no. 8, pp. 1591–1597, Aug. 2018, doi: 10.1109/TNS.2017.2787039.

[35] N. Kerboub *et al.*, "Temperature Effect on the Radioluminescence of Cu-, Ce-, and CuCe-Doped Silica-Based Fiber Materials," *IEEE Trans. Nucl. Sci.*, vol. 68, no. 8, pp. 1782–1787, Aug. 2021, doi: 10.1109/TNS.2021.3075481.

[36] I. Zghari *et al.*, "Effects of Measurement Temperature on Radioluminescence Processes in Cerium-Activated

Silica Glasses for Dosimetry Applications," *Sensors*, vol. 23, no. 10, p. 4785, May 2023, doi: 10.3390/s23104785.
[37] J. Vidalot *et al.*, "Optical Fiber-Based Monitoring of X-ray Pulse Series from a Linear Accelerator," *Radiation*, vol. 2, no. 1, Art. no. 1, Mar. 2022, doi: 10.3390/radiation2010002.
[38] F. Moretti, G. Patton, A. Belsky, A. G. Petrosyan, and C. Dujardin, "Deep traps can reduce memory effects of shallower ones in scintillators," *Phys. Chem. Chem. Phys.*, vol. 18, no. 2, pp. 1178–1184, Dec. 2015, doi: 10.1039/C5CP05711F.
[39] N. Kerboub *et al.*, "Radiation Induced Attenuation and Luminescence Study in Radioluminescent Optical Fibers," *IEEE Trans. Nucl. Sci.*, vol. 70, no. 8, pp. 1917–1924, Aug. 2023, doi: 10.1109/TNS.2023.3246239.
[40] F. Fricano *et al.*, "Reproducibility of Dose Rate Measurements with Radioluminescent Nitrogen-doped Optical Fibers," *IEEE Trans. Nucl. Sci.*, pp. 1–1, 2023, doi: 10.1109/TNS.2023.3263381.
[41] J. Vidalot *et al.*, "Mirror-Assisted Radioluminescent Optical Fibers for X-Ray Beam Monitoring," *IEEE Trans. Nucl. Sci.*, vol. 70, no. 4, pp. 575–582, Apr. 2023, doi: 10.1109/TNS.2023.3248680.